OSCILLATORY INTERACTION BETWEEN AN UNDEREXPANDED JET AND AN OBSTACLE IN THE PRESENCE OF A SUPERSONIC SHEATHED FLOW

G. F. Gorshkov, V. N. Uskov,
and A. P. Ushakov

UDC 532.525.2:533.6.
011.72

Nonstationary flows are amongst the most interesting phenomena in gas dynamics. A characteristic example is the oscillatory interaction between a supersonic jet and a flat obstacle, which explains the ongoing interest. This is evident from [1-6], which deal with a key aspect of oscillations: the forward and feedback channels that maintain the oscillations: Some suggest that the feedback mechanism is governed by sound waves propagating from the obstacle, which influence the mount of the jet [3], while others assert that the feedback is of shockwave type and occurs in the shock layer ahead of the obstacle [1, 5, 6].

External acoustic coupling may affect the frequency response, but we show here that it is not the principal effect causing nonstationary flow in the shock layer.

1. Experimental and Processing Methods. A supersonic wind tunnel was used with a cylinder system to supply air and an open working section. Figure 1 shows the general form of the apparatus and the pneumoelectric coupling to the tube. The coaxial supersonic flows were produced by the nozzle unit 2 attached to the main section 1 of the wind tube. The enclosing flow was provided by the annular nozzle, whose generators were provided by the cylindrical fitting 6 and the outer surface of the central nozzle body 4 and 5 (the shaping is considered below), while the jet was provided by the conical Laval nozzle 5. The working body (air having stagnation temperature T_0 = 290 K) was supplied to the peripheral nozzle directly from the main vessel, and to the central nozzle from the auxiliary vessel 7 via three pipes 8 and the three hollow sections 3. The planar obstacle 9 was a cylinder with flat end, diameter d = 28 mm, which was mounted in a holder on a coordinate table (Fig. 1c), which was fitted with an electric drive providing continuous displacement in the longitudinal direction at a velocity of 1 mm/sec. The center of the obstacle bore the LKh-611 piezoelectric pressure sensor with membrane working surface of 6 mm.

This design produced an almost uniform sheathing flow. The central nozzle body was shaped from calculations by the characteristic method [7], which dealt with the flow of gas from an annular nozzle (Fig. 1a) having a uniform solid flow at the input (on line AB), which was formed by the rectilinear wall BC and the stream line AD. Here AB and AE are the initial and final characteristics in the expanding flow, while ED is the characteristic beyond which the calculated flow velocity is attained. The shape of the central body was constructed for the geometrical parameter A = 0.76 (A = OA/OB < 1), but the actual profile AK differs from the theoretical one because the generator does not attain the point r = 0. It is necessary to interrupt the profile to locate the exit section of the central-jet nozzle. Tests with the peripheral nozzle showed that the pressure $P_{0\infty}/P_S \approx 14$ was attained at the end of the central nozzle with a given (monitored) outside pressure in the sheath space P_S and corresponded almost exactly to the calculated mode of flow from the angular nozzle (deviation from the calculated state $n_\infty = P_{a\infty}/P_S = 1$, in which $P_{a\infty}$ is the static pressure at the end of the peripheral nozzle for M_∞ = 2.365). The outside diameter of the peripheral nozzle (diameter of the sheath flow) was d_∞ = 120 mm. The central-jet nozzle was conical and had M_a = 2, d_a = 10 mm, d_* = 7.68 mm (d_a and d_* are the diameters at the outlet and in the critical section), while the thickness of the sharp edge at the end was about 0.4 mm, cone semivertex angle $\vartheta_a = 5°$.

We measured the total pressures in the peripheral system $P_{0\infty}$ and the central one P_0 and synchronized the recording equipment with a data-acquisition suite based on an Iskra 1256 minicomputer. The units were linked by a common interface. This acquisition system employed

Leningrad. Translated from Zhurnal Prikladnoi Mekhaniki i Tekhnicheskoi Fiziki, No. 4, pp. 50-58, July-August, 1991. Original article submitted January 5, 1990.

 0021-8944/91/3204-0512$12.50

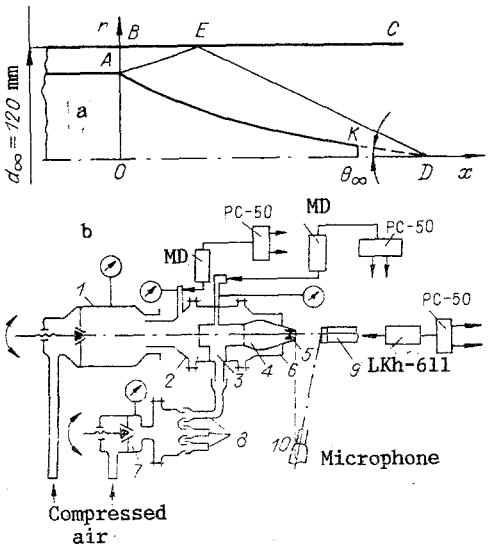

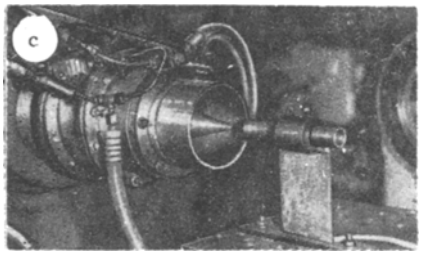

Fig. 1

combined processing. During the experiment, P_0 and $P_{0\infty}$ were input through the measurement chain constituted by the MD-T potentiometric sensor and were stored in the executive store, while the information on the pressure pulsations at the obstacle (in the surrounding space) $p(\tau)$ passed through the measuring circuits from the piezoelectric LKh-611 sensor (half-inch MK-221 capacitor microphone made by RFT, which was 1 m from the end of the nozzle and pointed towards the center of the obstacle: Fig. 1b, item 10), which worked with the 00 0011 microphone amplifier (RFT) and 01 021 noise meter (RFT), being then written in analog from to the NO 67 tape recorder (frequency range up to 40 kHz) without processing. The shock-wave pattern was recorded photographically with an RFK-5 camera (exposure 1/50 sec) working with an IAB-451 optical instrument. The measurement instant was identified on writting the data to tape by supplying a pulse from the control computer to one of the inputs. This was simultaneously the command pulse for the RFK-5. After the run, the P_0 and $P_{0\infty}$ were read out from the memory after conversion on the basis of the previous calibration to the printer as a record. The dynamic parameters on the tape were processed with an SK 4-72/2 narrow-band spectrum analyzer covering the range 0.05-20 kHz. The spectrograms were recorded with an Endim 622.01/1 XY recorder. The passband in the system from the sensor (microphone) to the tape recorder was better than 20 kHz. The measurement accuracy for P_0, $P_{0\infty}$, and $p(\tau)$ was 2-5%.

The pressures in the central and peripheral chambers were kept constant by means of control valves working with accuracy class 0.5 standard manometers (on the pressure plateau) in accordance with the working cycle, which involved the following sequence: bringing the central jet to working condition, starting up the peripheral nozzle, moving the obstacle, and recording the parameters. The interaction was examined with the obstacle continuously retreating downstream.

The parameters used were $M_a = 2$, $P_0/P_S = 51$, $M_\infty = 2.365$, $D_e = d_e/d_a = 2.8$, distance from the nozzle to the obstacle $H = h/r_a = 4.4\text{-}12.7$ (r_a radius at end of jet nozzle), $X = h/x_x = 0.595\text{-}1.716$ (x_x = 37 mm distance along the axis of the sheath jet from the end of the nozzle to the point of regular reflection for the hanging shock wave (Fig. 2)).

2. Results and Discussion. We first describe the free jet structure because it is important in controlling the flow conditions in the shock layer. Figure 2 shows schlieren photographs of the sheathed jet and the jet emerging in the sheath flow for constant stagnation pressure in the central system $P_0/P_S = 51$. The discrepancy $n_S = P_0/P_S = 6.52$ for the

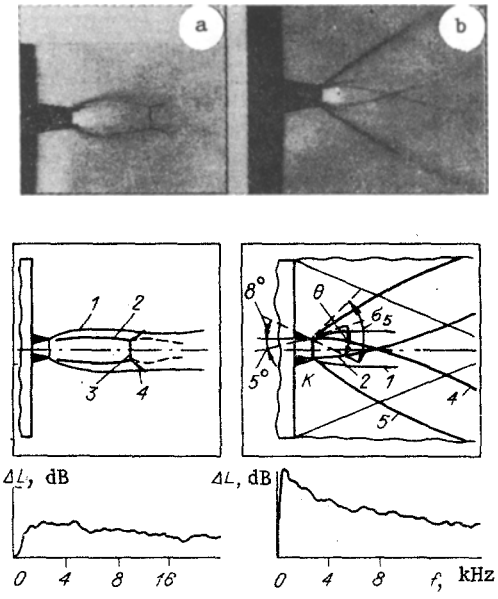

Fig. 2

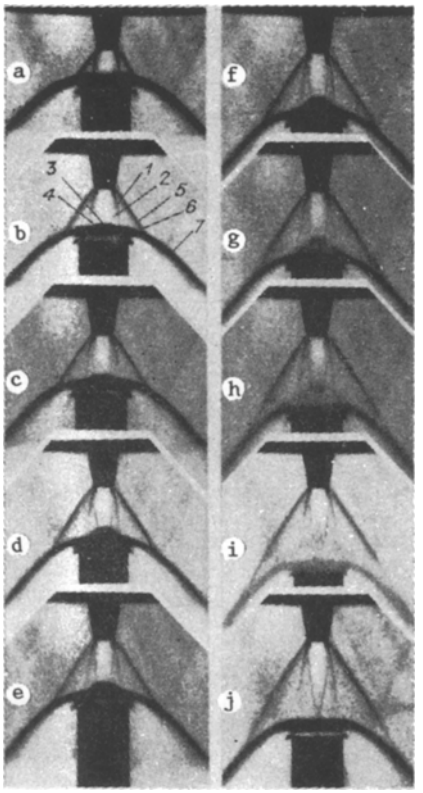

Fig. 3

sheathed jet corresponded to irregular reflection of the hanging shock wave 2 (Fig. 2a) from the symmetry axis with formation of the Mach disk 3. In the second case (Fig. 2b), for $P_{0\infty}/P_S = 14.75$ and a static pressure in the region of the nozzle edge K (Fig. 1a) $P_{a\infty}/P_S = 1.07$, the sheath flow encountered the flow from the conical nozzle at an angle of 13°, and the interaction between the flows gave rise to gas-dynamic discontinuities at point K, whose parameters can be calculated from local interference theory on the basis of the traditional dynamic compatibility conditions for shock waves [8]. With the given initial parameters for the flows, the following effects arose: shock wave 5 in the sheath flow and a negative-pressure wave ω in the jet, with the tangential discontinuity 1 between them, which is the boundary between the peripheral and central flows. The intensities of the shock wave $J_5 = P^0/P_{a\infty}$ and the negative-pressure wave $J_\omega = P^0/P_a$ should provide equal static pressures P^0 behind the waves on both sides of the tangential discontinuity, i.e.,

$$J_5 P_{a\infty} = P_a J_\omega. \tag{2.1}$$

There is a relation between the flow rotation angles β_5 and β_ω derived from the condition for collinerarity between the velocity vectors behind the shock front and in the negative-presure wave at K:

$$\beta_5 - \beta_\omega = 13°. \tag{2.2}$$

The known forms for $\beta_{\sigma,\omega}(J, M, \gamma)$ enable one to use (2.1) and (2.2) to calculate the corresponding J_5 and J_ω, e.g., $J_5 = 3.5$ and $J_\omega = 0.574$. These give the inclinations to the symmetry axis for the shock wave front ($\sigma_5 = 40.5°$) and the boundary of jet 1 ($\theta = 14.5°$), which agree well with the corresponding angles on the photographs. The central jet discrepancy derived from the static pressure behind shock front 5 $(n = P_a/P^0 = J_\omega^{-1} = 1.74)$, correspond to regular reflection of the hanging shock wave 2 from the symmetry axis when the jet flows into a sheathed space. This result agrees with [9], where it was observed that the central jet has very small Mach disk for $M_\infty > 2$.

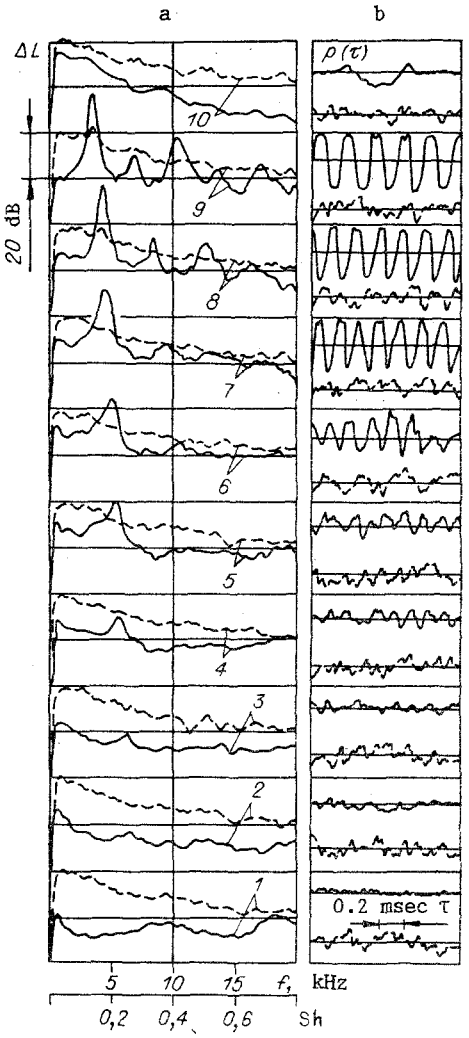

Fig. 4

The conditions for such a shock to arise are related to jet flow nonuniformity and parameters at the boundary. The sheath flow in our case was nonuniform up to edge K, while the jet emerged from the conical nozzle in an uncontrolled state. Those factors mean that the shock front 5 is curvilinear, as is the boundary of the jet 1, and also indicate variable static pressure along the boundary. The Mach numbers beyond the shock wave ($M_5^0 = 1.42$) and beyond the negative-pressure wave ($M_\omega^0 = 2.35$) alter substantially after the flows had interacted at the nozzle edge. The flow mixing rate at the boundary is dependent on the velocity difference and in turn governs the condition for the shock wave 4 reflected from the symmetry axis to pass into the outer flow. One can use solutions on the interaction of a shock wave with a tangential discontinuity [8] to analyze this, which shows that the intensity of the reflected discontinuity will be slight. This is probably the cause of the periodicity loss in the sheath jet that has several times been observed, e.g., in [9].

Detailed descriptions have been given [1-3] of the general pattern for a jet interacting with an obstacle of restricted size without a sheath flow. For given M_a and n, the interaction modes alter as the end of the nozzle recedes from the obstacle: 1) stationary radial flow, 2) nonstationary oscillatory state, and 3) a stationary state with unperturbed first branch point. If the jet strikes an unbounded obstacle [4], the nonstationary state (called the strong instability state) is followed by two others: flow with a central circulation zone and a second nonstationary state with weak instability. In the stationary flow state, the central shock wave recedes from the obstacle as the nozzle end recedes from it.

The sheath flow tansforms the flow pattern. This can be seen from the schlieren photographs in Fig. 3 ($M_a = 2$, $p_0/P_S = 51$, $M_\infty = 2.365$, $P_{0\infty}/P_S = 14.75$, $n = 1.74$) where 1 is the jet boundary, 2 the hanging shock wave, 3 the central shock wave, 4 the reflected shock wave, 5

the adjoint shock wave, 6 the receding shock wave, and 7 the resultant shock front, while parts a-j correspond to the following combinations of distances of the end of the nozzle from the obstacle: H = 5/X = 0.676; 6.1/0.824; 6.3/0.851; 6.9/0.932; 7.2/0.973; 7.5/1.014; 8.06/1.089; 8.6/1.162; 9.8/1.324; 10.2/1.378. The shock wave at the central part of the jet remains qualitatively unchanged (similar to the absence of a sheath flow). The flow retardation at the obstacle results in a central shock wave ahead of it, whose distance Δ from the obstacle is related to H for constant M_a and n as found above and described in [1-4]. However, the expanding jet from the surface of the obstacle itself represents an obstacle to the supersonic sheath flow. The flow around it at the periphery results in a receding shock wave, while the jet itself is deformed. The wave 5 from the nozzle edge is not altered (its inclination to the jet axis is unchanged) when the obstacle is present in the flow throughout the range in H. The intereference between shock waves 5 and 6 leads to the formation of a single gas-dyanamic discontinuity 7 at the edge of the sheath flow. The interaction between the central jet and the obstacle thus occurs in a narrow perturbed region bounded by the shock waves 5-7 and the surface of the obstacle. The above shock wave pattern corresponds to the stationary state of flow around the obstacle (subsequently termed the radial flow mode), which is characterized by a stationary shock wave pattern and the absence of pressure oscillations at the obstacle.

In some positions of the obstacle relative to the nozzle ($0.973 \leq X < 1.378$), the radial mode may be disrupted. An oscillatory type of interaction is set up (Fig. 3 e-i), which is characterized by oscillations in the shock wave pattern and the pressure at the obstacle $p(\tau)$. The nonstationary state arises, as in the absence of a sheath flow [2, 4] when the obstacle attains the point x_x from below: $X < 1$. However, one can establish the presence of the oscillations only from a careful comparison of the schlieren photographs with spectral measurements on the pressure pulsation at the obstacle and in the surrounding space (Fig. 4). The type of interaction is governed only by the position of the obstacle relative to the nozzle for fixed jet sheath flow parameters, so we consider the sequence of flow states as the obstacle recedes downstream.

Figure 4 shows the pressure pulsations spectrum for the center of the obstacle (solid lines), the acoustic pressure in the surrounding space (dashed lines), and the corresponding pressure waveform (b). The coordinates in the spectrograms are the relative level ΔL in the pressure pulsation in dB (ordinate) and the frequency f in kHz (abscissa). Parts 1-10 of Fig. 4 correspond to a-j in Fig. 3 (baffle receding from 1 to 10).

The Töpler photographs, spectrograms, and pressure measurements show that with radial flow (curves 2 in Fig. 3b and Fig. 4 a and b) the shock-wave pattern in the jet ahead of the obstacle is stable with a supersonic sheath flow, while the pressure-fluctuation spectra at the obstacle at the stagnation point and the acoustic pressure in the surrounding space are analogous to the spectrum for the continuous noise in a supersonic sheath jet (Fig. 2b). The pressure fluctuations at the obstacle and the acoustic pressure variations in the surrounding space (Fig. 4b) are of random type. That type of interaction persists to $X < 0{,}973$ $(4{,}4 \leqslant H < 7{,}2)$.

Any further increase in H perturbs the central shock wave ahead of the obstacle (with divergence as in Fig. 3d and e). A discrete component appears in the pressure-pulsation spectrum at the obstacle (basic frequency f_r = 5.4 or 5.3 on curves 4 and 5 in Fig. 4a), which exceeds slightly (by 5-7 dB) the level of the continuous noise from the jet. The pressure oscillations at the stagnation point are not completely deterministic (Fig. 4b), but there is a high proportion of low-frequency components in the spectrum. There is no discrete component in the pulsation spectrum for the acoustic pressure, and the oscillations are random (curves 4 and 5).

Further recession is accompanied by disruption of the shock pattern. The central wave ahead of the obstacle becomes diffuse (Fig. 3f-i), and developed oscillations occur. The oscillations in the central wave have high amplitude and comparatively low frequency. The discrete component in the pressure pulsation spectrum at the obstacle increases as H increases, and the maximum excess over the continuum level is 30-40 dB. The pressure oscillations at the stagnation point are deterministic and sinusoidal (curves 6-9, Fig. 4b). As H increases from 7.2 to 9.8, f_r decreases from 5.3 to 3.4 kHz. The acoustic-pressure spectra in the surrounding space still have no discrete component. The spectrograms are identical with those with the noise from a free sheath jet, while the acoustic pressure oscillations are random, as in the absence of coherent oscillations (curves 1-3), i.e., in the self-oscillation mode, the perturbations do not penetrate the supersonic sheath flow from the obstacle into the surrounding space and do not attain the edges of the nozzle, but instead are transported to downstream.

This regularity is very important (is a key feature) as regards the mechanism for nonstationary flow around the obstacle, as will become clear from the subsequent discussion. With developed oscillations, there is slight fuzziness in the closing shock fronts 6 and 7 (Fig. 3h and i, where they are somewhat diffuse in the photographs). However, the angles of inclination of them and of the shock wave 5 to the flow axis are almost as in radial flow (stationary). Beyond $X \geq 1.054$ ($H \geq 7.8$) the high-amplitude fundamental in the pressure is accompanied by oscillations of smaller amplitude at medium and high frequencies. The spectra contain not only the basic component (the first) but also several other discrete ones, which are much lower in level (e.g., curve 9 in Fig. 4 for $H = 9.8$: $f_r = 3.4$, $f_2 = 6.7$, $f_3 = 10.1$, etc.). That type of interaction (oscillatory) occurs with $0.973 \leq X < 1.378$ ($7.2 \leq H < 10.2$). Plots for the nonstationary state in the [1, 2] coordinates in the absence of the sheath flow show that if we take $n = 1.74$ for the jet, the area is that of self-oscillation.

Larger H ($X \geq 1.365$) result in a step to a stationary interaction. The pattern (Fig. 3j) is stable and corresponds to the positions of the shock waves in the first mode for the free sheath jet (Fig. 2b), while an additional shock arises ahead of the obstacle, which passes continuously into shock front 6. The pressure pulsation spectra for the obstacle and the surrounding space contain no discrete components, and the oscillations themselves are random (Fig. 4, curves 10). The pressure spectra are similar to the noise spectrum for the free sheath jet (Fig. 2b). That type of interaction occurs for $1.378 \leq X \leq 1.716$ ($10.2 \leq H \leq 12.7$). When the obstacle moves towards the nozzle (H varying from 12.7 to 4.4), one gets the same set of modes but in the opposite sequence: a state with unperturbed first mode, oscillations, and radial flow. However, there is hysteresis with respect to H, since the end of the oscillations (start for motion away from the nozzle) occurred at H somewhat less than that given above.

The parameters in the system represented by the central wave and the obstacle affect the obstacle, namely as H increases within the oscillation range, there is a reduction in f_r, and the same effect is produced by increasing n and M_a [1, 2, 4]. There are several published approaches (which do not differ greatly) [1, 2] to choosing the universal similarity parameters for the frequency characteristics. For example, a series of $Sh_a \sqrt{M_a} = f(H, D_e)$ universal curves has been suggested for the dimensionless frequency ($Sh_a = f_r d_a / U_a$ is the Strukhal number, which is calculated from the gas speed at the end of the nozzle U_a) [1]. However, each n then corresponds to a distinct part of the curve. In [2], f_r was derived from a $f_r d_a = f(\Delta, r_a)$ approximation in which Δ is the distance around which the central wave oscillates ahead of the obstacle (the mean position of what wave, which can [1, 2] be determined as though the oscillations were absent). That approximation can be transformed if one introduces the speed of sound a_0 in the braked flow. Then $Sh_0 = f_r d_a / a_0 = f(\Delta / d_a)$, which incorporates the effects of the obstacle size and other factors (via Δ) and which is more general than for example the [1] formula. However, it also does not adequately incorporate the geometry (particularly the transverse dimensions) of the region in the oscillating wave. One expects that as the transverse dimensions of the jet are proportional to $\sqrt{n}$, introducing as a measure of the diameter of this region (a suggestion due to Favorskii) will enable one not only to reduce the spread in the measured points around some average curve but also to derive a universal relationship corresponding to the physical model.

A similar analysis can be applied to nonstationary state for a bounded obstacle in order to extend the existing results (with an accuracy of about 10%) by means of a straight line (Fig. 5)

$$Sh_r^{-1} = \frac{a_0}{f_r d_a \sqrt{n}} = 3{,}6 \frac{\Delta}{d_a \sqrt{n}} + 1{,}3, \qquad (2.3)$$

which is a linear function of the oscillation wavelength $\lambda = a_0 / f_r = a_0 t$ (t is the period) and of the geometrical parameters Δ and $d_a \sqrt{n}$: $a_0 t = 3{,}6\Delta + 1.3 d_a \sqrt{n}$.

Figure 5 employs our data with an without the sheath flow together with the [1, 2, 4] results for the absence of a sheath flow. Parts 1-15 correspond to the following parameter combinations: 1-5 ($M_a = 2$; $n_s = 2.67$-6.52; $D_e = 2.8$; $d_a = 10$ mm without sheath flow), 6 (2; 4.06; 2.15; 20 [4]), 7 (2; 3; 1; 30 [1]), 8-10 (1.5; 3-16.5; 2.5; 20 [2]), 11, 12 (1; 4-13.5; 2.5; 20 [2]), 13, 14 (1.5; 2.2-5.2; 1.5; 40 [2]) and 15 (2; 1.74; 2.8; 10 sheath flow), while the line is by calculation from (2.3). Here Δ was taken either from direct measurements or was determined from the [2, 4] formulas.

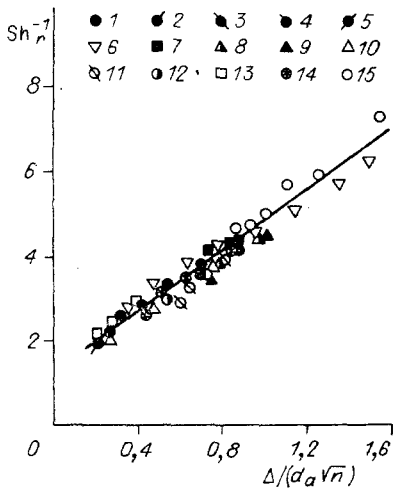

Fig. 5

These measurements show that oscillations arise when there cannot be feedback from acoustic waves propagating from the surrounding space to the edge of the nozzle. The causes of the nonstationary state and the mechanism that maintains it are related to processes in the shock layer ahead of the obstacle. This is particularly so for the shock-wave structures formed by interference between gas-dynamic discontinuities arising ahead of the obstacle when the jet is braked and caused to diverge, which interact with discontinuities in the jet and the sheath flow. In particular, the triple shock-wave configuration arising from the interaction of the central wave with the hanging shock wave leads to a substantially nonuniform entropy distribution in the central and peripheral parts of the shock layer. Calculations show that this nonuniformity becomes more marked as the triple configuration recedes from the exit nozzle section. At the same time, the gas flow in the high velocity peripheral stream increases, as does the inclination to the baffle in the tangential discontinuity arising from the triple point. That situation tends to shut off the gas passing through the central shock, an effect that is accentuated by the sheath flow, which alters the conditions for the jet spread over the obstacle. The central flow shut off by the low-entropy peripheral one results in pertubations propagating from the obstacle to the central shock wave through the central flow (feedback channel) and from the shock waves to the obstacle (forward channel) [6]. The [5] shock-wave scheme, which is qualitatively confirmed by numerical calculations [6], can also occur with a supersonic sheath flow.

LITERATURE CITED

1. G. V. Naberezhnova and Yu. N. Nesterov, "Unstable interaction of an expanding supersonic jet with an obstacle," Trudy TsAGI, No. 1765 (1976).
2. A. V. Solotchin, "Instability in a supersonic under-expanded jet encountering an obstacle," In: Jet-Flow Gas Dynamics and Acoustics [in Russian], Inst. Theor. Prikl. Mekh. Sib. Otd. Akad. Nauk (IPTM SO AN) SSSR, Novosibirsk (1979).
3. V. N. Glaznev, "A semiempirical theory of discrete-frequency generation in a supersonic under-expanded jet striking an obstacle," Izv. Akad. Nauk SSSR, MZhG, No. 6 (1981).
4. E. I. Sokolov and V. N. Uskov, "Interaction of an axisymmetric jet with an obstacle and a supersonic countercurrent," In: Jet and Detached Flows [in Russian], Mosk. Gos. Univ., Moscow (1985), Part 3.
5. B. G. Semiletenko, B. N. Sobkolov, and V. N. Uskov, "A scheme for shock-wave processes in the unstable interaction of a jet with an obstacle," Izv. Sib. Old. Akad. Nauk SSSR, Ser. Tekh. Nauk, No. 13, Issue 3 (1972).
6. V. N. Uskov, V. V. Tsymbalov, and E. N. Tsymbalova, "Numerical solution for nonstationary interaction of a supersonic jet with an obstacle," In: Simulation Otd. Mechanics [in Russian], Vol. 1 (18), No. 6, VTs, ITPM SO AN SSSR, Novosibirsk, 1987.
7. O. N. Katskova, "Calculations on annular supersonic nozzles and diffusors," in: Computational Mathematics [in Russian], No. 3, Akad. Nauk SSSR, Moscow (1958).
8. V. N. Uskov, "Interference between stationary gas-dynamic discontinuities," in: Supersonic Gas Jets [in Russian], Nauka, Novosibirsk (1983).
9. V. S. Avduevskii, É. A. Ashratov, A. V. Ivanov, and U. G. Pirumov, Supersonic Nonisobaric Gas Jets [in Russian], Mashinostroenie, Moscow (1985).